FLEXIBLE ELECTRONICS

Universal assembly of liquid metal particles in polymers enables elastic printed circuit board

Wonbeom Lee[1]†, Hyunjun Kim[1]†, Inho Kang[2], Hongjun Park[3], Jiyoung Jung[4], Haeseung Lee[1], Hyunchang Park[1], Ji Su Park[1], Jong Min Yuk[1], Seunghwa Ryu[4], Jae-Woong Jeong[2], Jiheong Kang[1]*

An elastic printed circuit board (E-PCB) is a conductive framework used for the facile assembly of system-level stretchable electronics. E-PCBs require elastic conductors that have high conductivity, high stretchability, tough adhesion to various components, and imperceptible resistance changes even under large strain. We present a liquid metal particle network (LMP_{Net}) assembled by applying an acoustic field to a solid-state insulating liquid metal particle composite as the elastic conductor. The LMP_{Net} conductor satisfies all the aforementioned requirements and enables the fabrication of a multilayered high-density E-PCB, in which numerous electronic components are intimately integrated to create highly stretchable skin electronics. Furthermore, we could generate the LMP_{Net} in various polymer matrices, including hydrogels, self-healing elastomers, and photoresists, thus showing their potential for use in soft electronics.

Stretchable electronics with high stretchability and high toughness are essential for soft robotics (*1*, *2*), skin electronics (*3*, *4*), and implantable electronics (*5*, *6*). Substantial progress has been made in intrinsically stretchable conductors. High metallic conductivity with rubber-like stretchability has been successfully achieved in conductive polymers (*7*) and nanocomposites (*8*–*12*). However, certain critical challenges, including the inevitable change in electrical resistance during stretching and difficulty in achieving long-term cyclic stability and strong interfacial bonding with electronic components, remain. Hence, an elastic printed circuit board (E-PCB) has not been realized without structure engineering (*13*).

Room-temperature liquid metals (LMs) have received considerable attention as elastic conductors because of their metallic conductivity and extreme deformability. Gallium-based LMs have been studied for elastic conductors through various approaches, including dispersing LM particles (LMPs) in an elastomer (*14*, *15*), coating LM on a porous polymer matrix (*16*), mixing LMPs with a solid conductive filler composite (*17*, *18*), doping LMPs in a polymer matrix (*19*), and forming a biphasic LM structure (*20*). However, LM-based conductors suffer from leakage issues under external mechanical stimuli, which limit their reliability, uniformity, and stability.

[1]Department of Materials Science and Engineering, Korea Advanced Institute of Science and Technology (KAIST), Daejeon 34141, Republic of Korea. [2]School of Electrical Engineering, Korea Advanced Institute of Science and Technology (KAIST), Daejeon 34141, Republic of Korea. [3]Center for Nanomaterials and Chemical Reactions, Institute for Basic Science (IBS), Daejeon 34141, Republic of Korea. [4]Department of Mechanical Engineering, Korea Advanced Institute of Science and Technology (KAIST), Daejeon 34141, Republic of Korea.
*Corresponding author. Email: jiheongkang@kaist.ac.kr
†These authors contributed equally to this work.

We report a universal synthetic route for highly conductive and mechanically tough LMP-based conductors without the LM leakage issue (Fig. 1). Our LM conductor includes a long-range assembled network of LMPs (LMP_{Net}) and a tough elastomeric matrix. The percolation structure and deformation mechanisms of the LMP_{Net} led to high conductivity, outstanding toughness, and imperceptible resistance changes under large deformation (Fig. 1C). The LMP_{Net} is composed of a network of large LMPs (average size of 2 to 3 μm) as the main framework and smaller LMPs (average size of 100 nm, denoted as LMP_{nano}) as network interconnectors (Fig. 1B and figs. S1 to S3). When the LMP_{Net} is stretched, the micrometer-sized LMPs deform into ellipsoidal structures, whereas the LMP_{nano} interconnectors remain intact similarly to solid particles (Fig. 1C and figs. S1 and S2). Thus, particle–particle contacts could be preserved under large strain, resulting in negligible resistance changes under large strain (>4000%).

The LMP_{Net} could be formed with high uniformity and reliability over a large area (fig. S4). This allowed us to predict the electrical resistance of the lines and design an E-PCB, in which various electronic components, including integrated circuit (IC) chips, resistors, transistors, and capacitors are assembled with tough interfacial adhesion (Fig. 1D).

As illustrated in Fig. 1, A and B, and fig. S5, the formation of the LMP_{Net} in a polymer matrix was accomplished in two steps: First, an LMP–polymer composite was formed, and then the LMP_{Net} formation was induced. To prepare micrometer-sized LMPs, we applied an acoustic field to the room-temperature LM alloy (eutectic gallium indium, EGaIn) (1.35 g) in acetone (30 ml) at an amplitude of 63.4 μm (44%) for 20 min, using a probe sonicator in water. The solvent was decanted after centrifugation for 30 min at 2200 rpm. The sedimented LMPs were mixed with a thermoplastic elastomer, polyurethane (PU) dissolved in dimethylacetamide (DMAc, 200 mg/ml), by using a THINKY mixer for 10 min. Scanning electron microscopy images and the size distribution of the LMP samples processed by various acoustic field application times are shown in fig. S6. Thereafter, the LMP–PU ink was printed on a PU substrate, and the printed lines were annealed at 80°C for 24 hours to completely remove the residual solvent (fig. S7).

The as-printed lines are insulating because of the large interparticle distance of LMPs in the polymer matrix that is induced by the electrostatic repulsion of native oxides on LMPs (*21*) (Fig. 1B, left). Generally, LMP-based conductors require an activation (sintering) step to interconnect the LMPs and achieve high conductivity. Various activation methods, such as external mechanical force application (*14*, *15*), high-temperature sintering (*20*), and laser sintering (*22*), have been reported. These methods rupture the native oxide of LMPs and cause a substantial amount of LM to leak to other LMPs, thereby forming percolation pathways. These methods have limitations in the reliability, uniformity, and mechanical robustness of circuit lines. During the activation, a large amount of LM emerges from the surface of conductive lines and disrupts other lines (fig. S8).

We devised an alternative method for forming a highly conductive LMP assembled network in the polymer matrix without LM leakage. This method involves acoustic field application to as-printed LMP lines. For this, we chose water as the medium to avoid unwanted damage to the printed lines or temperature increase. When an acoustic field was applied for 30 s, we observed the formation of nanosized LMP (LMP_{nano}) between the original micrometer-sized LMPs (Fig. 1B and figs. S1 to S3), resulting in the interconnection of the LMPs with LMP_{nano}, that is, the formation of the LMP_{Net}.

We investigated the electrical characteristics of the LMP_{Net} depending on the LM volume fraction in the composite. The as-printed LMP conductor was insulating, even at a high LM content, and required an acoustic field to form a conductive LMP_{Net} (Fig. 2A). The conductivity of the LMP_{Net} increased with an increase in the LM volume fraction in the composite, and it reached 2.10×10^6 S/m at 74.4 vol % of the LM (Fig. 2A and fig. S9). Considering the volume fraction of the polymer in the composite and the electrical conductivity of the pure LM, the resultant conductivity nearly reached the theoretical effective conductivity calculated by using the relationship $\sigma = \sum f_A \sigma_A$, where f is the volume fraction of the conductive material and σ is the electrical conductivity of the conductive component (Fig. 2A and fig. S10) (*23*). This result suggests that a nearly

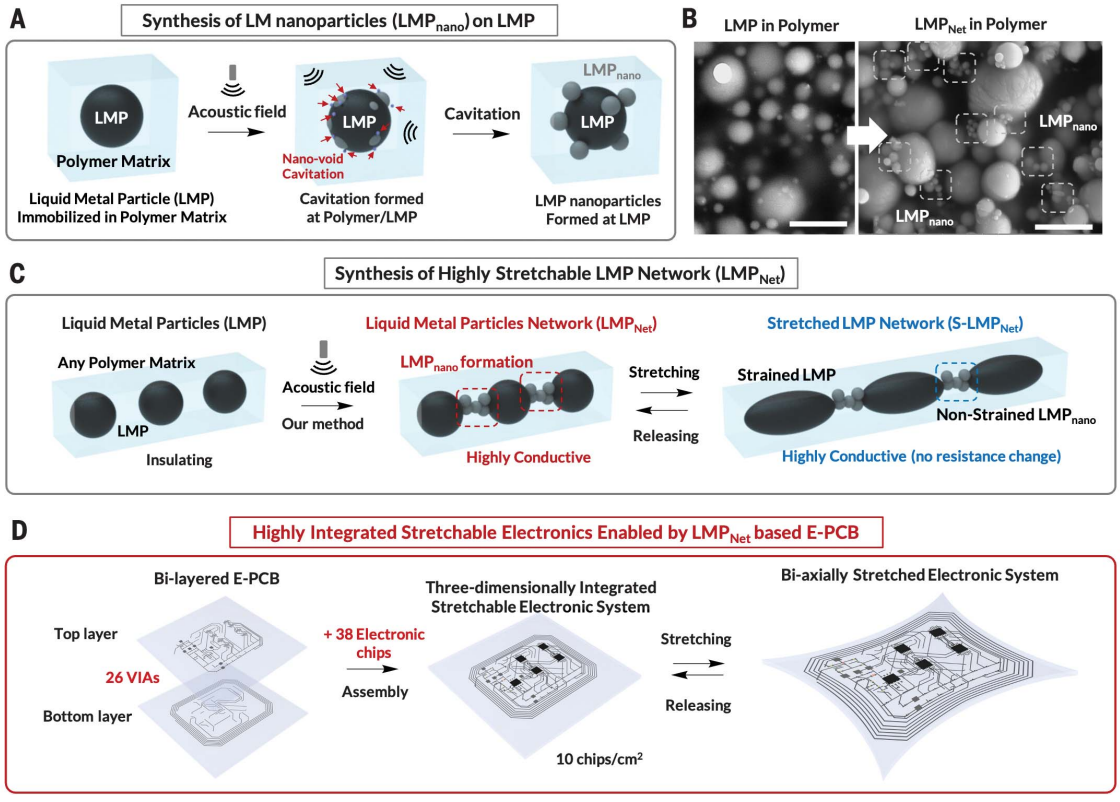

Fig. 1. Formation of a liquid metal particle network in a polymer and its application for elastic printed circuit boards. (**A**) Schematic of the formation of liquid metal nanoparticles (LMP$_{nano}$) at the surface of existing micrometer-sized liquid metal particles (LMPs) via acoustic field application. (**B**) Scanning electron microscopy images of the LMPs and LMP network (LMP$_{Net}$) formed in the polymer, which reveal that LMP$_{nano}$ species are formed at the surface of the original LMPs. Scale bars, 3 μm. (**C**) Schematic illustration of the formation of a highly conductive LMP$_{Net}$ and the distinctive behavior of the elastic LMP$_{Net}$ derived from the differences in the sizes of the original LMP and LMP$_{nano}$, resulting in negligible resistance change during stretching. (**D**) Schematic illustration of the elastic multilayered printed circuit board based on the LMP$_{Net}$ and the assembly of integrated stretchable electronics.

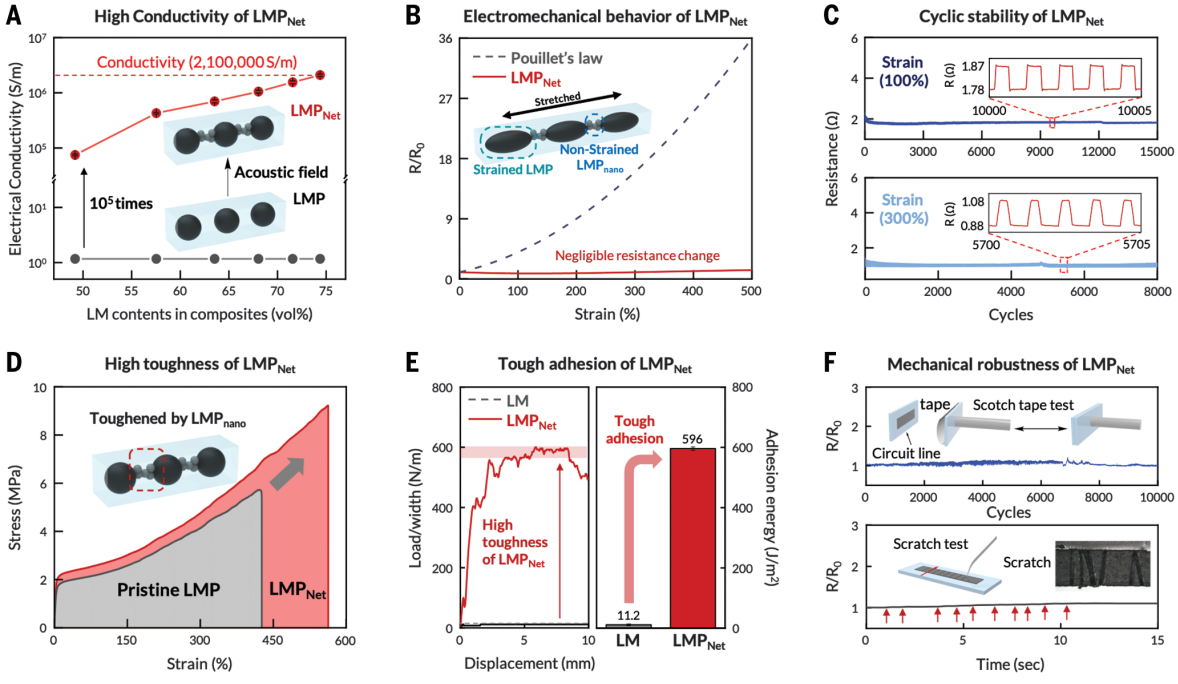

Fig. 2. Electrical and mechanical properties of LMP$_{Net}$. (**A**) Electrical conductivity of the LMP–polymer composite as a function of the liquid metal content before and after the LMP$_{Net}$ formation; the electrical conductivity of the LMP$_{Net}$ reached 2.10 × 10^6 ± 9.8 × 10^4 S/m (n = 3, where n is the number of samples that are used to generate statistical data). (**B**) Relative resistance changes of the LMP$_{Net}$ under uniaxial strain of up to 500% (red line, R/R_0 = 1.33), and theoretical prediction based on an incompressible spherical conductor [gray dot, $R/R_0 = (1+\epsilon)^2$, where ϵ is the applied strain]. (**C**) Relative resistance changes of the LMP$_{Net}$ line during 15,000 cycles of stretching at 100% strain (top, dark blue) and 8000 cycles of stretching at 300% strain (bottom, pale blue). The insets show a detailed resistance response of the conductor to the applied strain. (**D**) Stress–strain curves of the LMP–polymer (gray) and LMP$_{Net}$–polymer (red) composites. The mechanical strength increased by 160% and the toughness increased by 190% when the LMP$_{Net}$ was formed. (**E**) Interfacial adhesion strength of the pure LM and LMP$_{Net}$ on a surface-functionalized substrate. The interfacial adhesion strength of the LMP$_{Net}$ (596 ± 5.6 J/m^2, n = 3, where n is the number of samples that are used to generate statistical data) on the surface-functionalized substrate is more than 5300% higher than that of the pure LM (11.2 ± 3.2 J/m^2, n = 3, where n is the number of samples that are used to generate statistical data). (**F**) Relative resistance changes of the LMP$_{Net}$ under external stimuli, Scotch-taping (top), and scratching (bottom), which demonstrate the mechanical and electrical robustness of the LMP$_{Net}$.

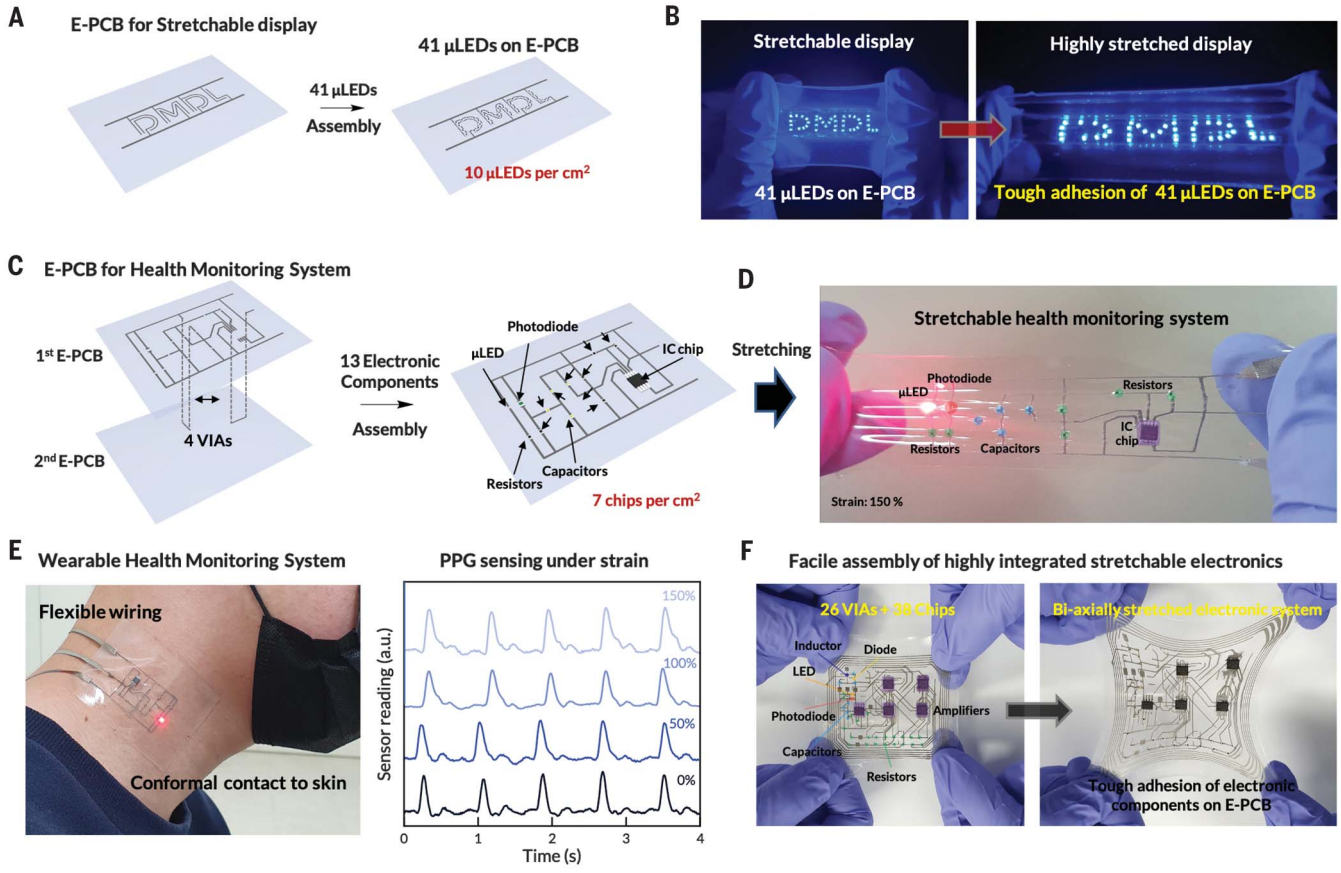

Fig. 3. LMP_{Net}-based E-PCB. (**A**) Schematic illustration of the circuit line and an LED array assembled using the LMP_{Net} for a stretchable display. (**B**) Optical images of the LED array reading "DMDL" at rest (left) and under 100% strain (right). (**C**) Schematic illustration of the circuit lines, VIAs, and electronic components assembled using the LMP_{Net} for a stretchable health monitoring system. (**D**) Optical image showing the operation of a photoplethysmography (PPG) sensor before and after stretching by 150%. (**E**) Optical image of the PPG sensor attached to human skin (left) and the normalized reading of the PPG sensor as a function of the strain (0, 50, 100, and 150% strain) applied to the PPG sensor circuit board (right). (**F**) Optical image of a stand-alone integrated stretchable electronic system (left) and biaxially stretched electronic system (right). This system includes 26 VIAs and 38 electronic components.

defect-free percolation pathway was formed by the assembly of the LMPs in the polymer matrix. Although the LMP_{Net} is based on a zero-dimensional particle structure, its electrical conductivity is higher than those of the previously reported elastic printable conductors (fig. S11) (*7*, *9*, *10*, *16*–*18*, *20*). The LMP_{Net} exhibited zero resistance change at 100% strain (R/R_o = 1.00) and excellent electromechanical decoupling at 600, 2000, and 4100% strain (R/R_o = 1.41, 5.18, and 20.8, respectively) (Fig. 2B and fig. S12). It has excellent environmental stability (phosphate-buffered saline, 16 weeks), thermal stability (fig. S13), and high cyclic stability (15,000 cycles at 100% strain, 8000 cycles at 300% strain, and 1200 cycles at 500% strain) (Fig. 2C and fig. S14). We investigated the effects of the strain rate and LM volume fraction on the electromechanical behavior of the LMP_{Net} conductor. The LMP_{Net} exhibits a stable electrical performance during dynamic stretching, regardless of the strain rate (fig. S15) and the LM volume fraction (fig. S16). We also confirmed its imperceptible change in the resistance even under biaxial stretching (fig. S17).

According to Eshelby's theory, LMPs in an elastomeric matrix deform their structures when a strain is applied. This feature allows much better electromechanical responses from LMP-based conductors than from conventional rigid conductive filler-based conductors (fig. S18). The electromechanical properties of our LMP_{Net} conductor result from not only the deformation of the LMPs but also the structure of the assembled LMP network. The deformation of LMPs is size dependent, with nanosized LMP_{nano} mimicking the behavior of solid particles (*24*). We performed theoretical simulations and confirmed this size-dependent deformation of LMPs in the polymer (fig. S19) (*24*–*26*). When LMP_{Net} was stretched, we observed that large LMPs deformed to ellipsoidal structures and the LMP_{nano}'s between large LMPs were intact (fig. S1). The dissimilar deformation of the LMPs of two different sizes enables the realization of a mechanically and electrically resilient percolation network (Fig. 1C).

To understand the impact of the LMP_{Net} on the mechanical properties, we performed mechanical tests on three samples: pure PU, LMP–PU, and LMP_{Net}–PU. In contrast with rigid conductive fillers, LMP inclusions in PU, which have zero Young's modulus, make the LMP–PU composite softer (fig. S20). However, the deformation and crack-bridging effect of the LMP substantially toughen the polymer matrix (*27*). We investigated how the LMP_{nano} affects the mechanical properties of the composite. As discussed above, LMP_{nano} behaves like a solid particle in PU and thus has a stiffening effect on the PU matrix (Fig. 2D and fig. S21). LMP_{nano} also improved the stretchability and toughness of the composite (Fig. 2D) because of the additional energy dissipation mechanism facilitated by the reversible assembly of the LMP_{Net} (fig. S22).

The interfacial adhesion problem of LMP conductors with rigid electronic chips is severe in E-PCB. Owing to the low toughness of LMP, electronic chips are easily delaminated from conductive lines by cohesive failure when stretched.

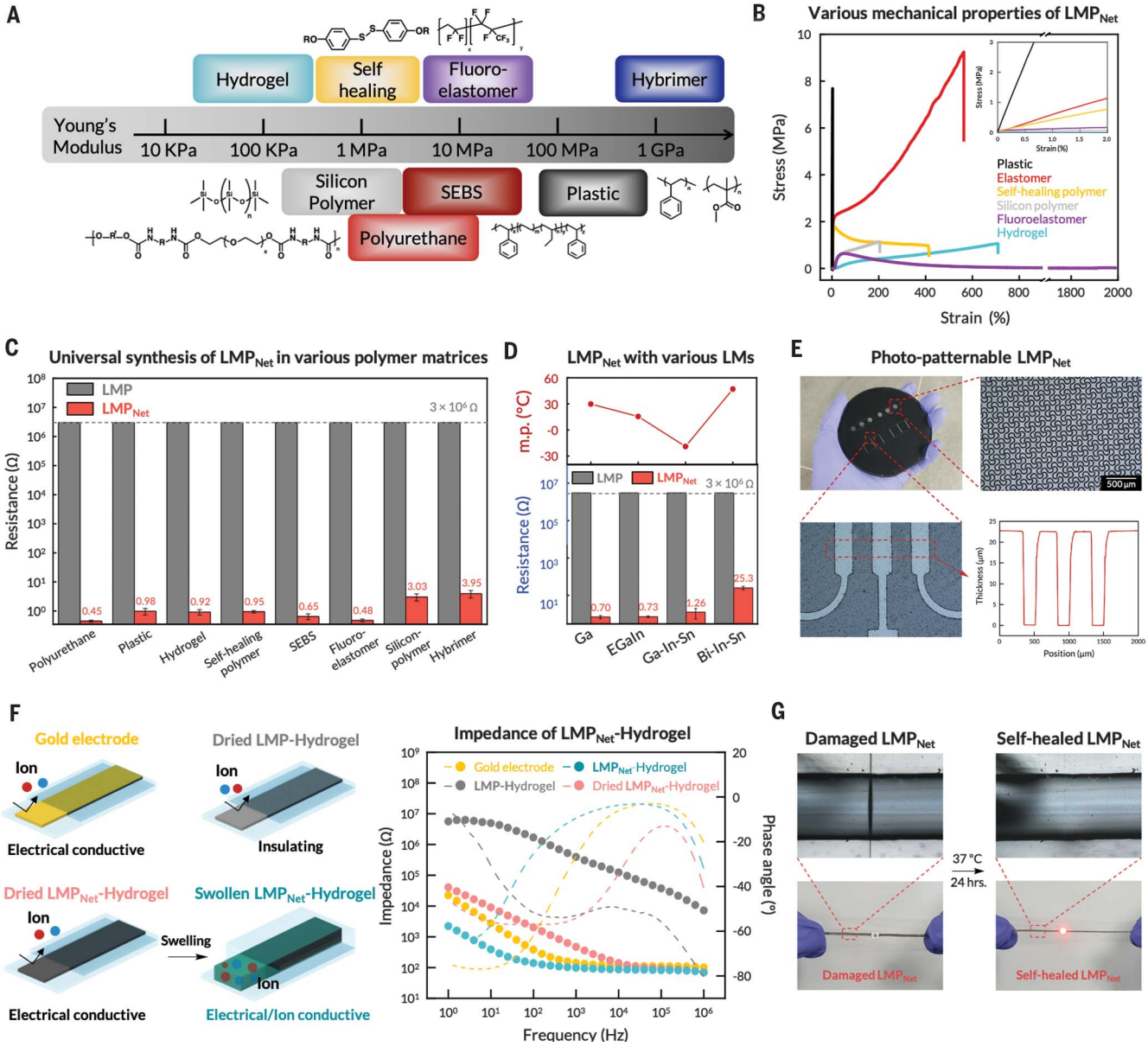

Fig. 4. LMP$_{Net}$ in various polymers. (**A**) Young's modulus of various polymer matrices used for LMP$_{Net}$ formation. (**B**) Stress–strain curves of the LMP$_{Net}$ formed in various polymers (plastic, elastomer, self-healing polymer, silicon-based polymer, fluoropolymer, and hydrogel); the data reveal that the mechanical properties can be tuned by choosing an appropriate polymer. (**C**) Resistance of the LMP–polymer and LMP$_{Net}$–polymer composites based on diverse polymer matrices. The LMP$_{Net}$ shows low electrical resistance (<5 ohms), regardless of the host matrix (n = 4, where n is the number of samples that are used to generate statistical data). (**D**) Melting point (top) and resistance (bottom) of the LMP$_{Net}$ formed from four types of liquid metal alloys with different compositions; the data demonstrate that various types of metals with low melting points can also be used to form the LMP$_{Net}$ (n = 4, where n is the number of samples that are used to generate statistical data). (**E**) Digital image (top left), optical microscopy image (top right, bottom left), and thickness profile (bottom right) of a photopatterned LMP$_{Net}$. (**F**) Schematic illustration of various electrodes (left) and their impedance spectra (right); gold electrode (yellow), dried LMP–hydrogel (gray), dried LMP$_{Net}$–hydrogel (red), and swollen LMP$_{Net}$–hydrogel (blue). Swollen LMP$_{Net}$–hydrogel exhibits the lowest impedance owing to the penetration of ions into the hydrogel (left). (**G**) Optical microscopy images (top) and digital images (bottom) of a damaged and self-healed LMP$_{Net}$.

Our LMP$_{Net}$–PU lines afford high interfacial adhesion energy (596 J/m^2) with various engineered surfaces. This can be attributed to the adhesion properties of PU and efficient energy dissipation facilitated by the LMP$_{Net}$ (Fig. 2E and fig. S23). As demonstrated in fig. S24 and movie S1, a commercial micro–light-emitting diode (μLED) bonded to LMP$_{Net}$–PU lines exhibited stable performance under dynamic deformation even without the aid of an encapsulation layer.

One of the major challenges of the reported LMP-based conductors is the leakage of the LM owing to the continuous rupture of LMPs by mechanical stimuli. For example, upon scratching or stretching, several LM droplets emerged from the conductive lines (fig. S8). By contrast, no LM leakage could be observed from our LMP$_{Net}$ conductive lines, and no degradation of the electrical properties was noted upon scotch-taping, scratching, or stretching the conductive lines (Fig. 2F and fig. S25). The mechanical robustness of the LMP$_{Net}$ can be attributed to both the high toughness of the LMP$_{Net}$–PU and the relatively small size of the LMPs. In this study, we used LMPs with an average size of 2 μm as the main component of

the LMP_{Net}. In previously reported LMP systems (*14*, *15*, *19*), large LMPs (more than 10 μm) were used to achieve high conductivity. We experimentally confirmed the LM leakage issue in the case of an LMP_{Net} with LMP sizes of >5 μm (fig. S8). Notably, we achieved a high conductivity of the LMP_{Net} even with 2-μm LMPs (Fig. 2A).

To understand how LMP_{nano} is generated by an acoustic field, we studied multiple possible mechanisms (figs. S26 to S27). The acoustic field can generally be thought to cause a temperature increase or the collapse of nanobubbles on the surface of the printed lines (*28*). We did not observe any evolution of the percolation network when the LMP lines were annealed at 150°C for 1 day (fig. S28A), indicating that the LMP_{nano} formation is not due to temperature increase. Further, we could also exclude the effect of nanobubbles formed in the medium and their collapse at the water/line interface through two experiments. If the network formation is a surface event, a thickness dependence of the LMP_{Net} formation is expected. However, the LMP_{Net} could be generated even in a 60-μm-thick film with the same electrical conductivity as that of a 20-μm-thick film (fig. S29). We covered the LMP lines with a thick PU film and applied an acoustic field. We observed the successful formation of the LMP_{Net}, suggesting that it was not a surface event (fig. S28B).

We hypothesize that the LMP_{Net} formation occurs in three distinct steps (Fig. 1A and fig. S30). First, the acoustic energy is transferred from the probe sonicator to the composite via the water medium. Then, the acoustic energy accumulates at the LMP/polymer/LMP interface. As the polymer is acoustically transparent, the acoustic wave energy can freely travel and reach the bottom part of the polymer film (table S1). By contrast, LMPs have a high acoustic impedance and mostly reflect the wave energy. Owing to the large difference in acoustic impedance between the polymer and LMP, the wave energy mostly accumulates at the LMP/polymer/LMP interfaces. We confirmed this possibility through finite element simulation using a simple model (fig. S31). The accumulated acoustic energy starts to form nanobubbles (cavitation) at the LMP/polymer/LMP interface. The final step is the generation of LMP_{nano} from the original LMPs by the collapse of the nanobubbles (Fig. 1A). That is, LMP_{nano} is generated directly from the LMPs without complete rupture of LMPs. This event occurs inside the LMP–polymer composite, wherein the LMPs are immobilized. Therefore, LMP_{nano} forms efficiently and interconnects the LMPs without moving to other free spaces in the polymer matrix (fig. S1). Thus, a highly conductive LMP_{Net} was formed through these steps, in which large LMPs were compactly assembled by LMP_{nano} with an interparticle distance of less than 2 nm (fig. S3B). A similar outcome can be expected if LMP_{nano} is mixed with LMPs in the conductive ink. However, we could not observe any evolution of the percolation network, which indicated that LMP_{nano} did not interconnect the LMPs (insulating) (fig. S32).

To realize E-PCB, we confirmed the processability of the LMP_{Net} conductor. Our LMP_{Net} conductor provides an excellent platform via a printing process for the fabrication of E-PCB. We confirmed excellent printability, stretchable vertical interconnect accesses (VIAs), and chip-bonding processes (figs. S33 to S35). As a proof of concept, we fabricated bi-layer E-PCB and assembled integrated electronics, including a μLED array (Fig. 3, A and B; fig. S36; and movie S2) and a photoplethysmography (PPG) sensing wearable device (Fig. 3C and fig. S37). As shown in Fig. 3, B, D, and E, they can exhibit stable electrical performance under dynamic stretching. In addition, we fabricated highly integrated skin electronics, in which 26 VIAs and 38 chips were assembled, and confirmed their robustness under biaxial stretching (Fig. 3F and fig. S38).

Our acoustic field–based LMP_{Net} synthesis should apply to most polymer matrices. We successfully formed LMP_{Net} in more than 15 different polymers with various chemical and mechanical properties (Fig. 4, B and C; figs. S39 and S40; and table S2). We also confirmed the formation of LMP_{Net} using other LM alloys with different melting temperatures and compositions (Fig. 4D). All the LMP_{Net} systems exhibited high conductivity, regardless of the polymer and LM.

The LMP_{Net} could also be formed in a photoresist (SU-8), which enabled the high-resolution patterning of LMP_{Net} conductive lines (Fig. 4E and fig. S41). We observed unusual electrochemical features in a LMP_{Net}–hydrogel. We obtained the impedance spectrum of the LMP_{Net}–hydrogel in the frequency range 1 to 1×10^6 Hz and observed that our LMP_{Net}–hydrogel electrode exhibits one order of magnitude lower impedance than Au electrodes in the low-frequency range (Fig. 4F and figs. S42 to S44). This observation results from the high dual conductivity (electronic and ionic conduction) and high surface area of the LMP_{Net} in the hydrogel. The initial dry LMP_{Net}–hydrogel was only electronically conductive, whereas the sample swollen with electrolyte solution exhibited mixed electron and ion conduction, leading to extremely low impedance (*6*). Considering the biocompatibility of EGaIn and hydrogel matrix, our LMP_{Net}–hydrogel can be designed as an implantable electrode. Moreover, we formed an LMP_{Net} in a self-healing elastomer (SHE) (Fig. 4C) and investigated its mechanical and electrical self-healing properties (*29*, *30*). The LMP_{Net}–SHE could autonomously restore its mechanical and electrical properties when damaged (Fig. 4G).

REFERENCES AND NOTES

1. S. I. Rich, R. J. Wood, C. Majidi, *Nat. Electron.* **1**, 102–112 (2018).
2. D. Rus, M. T. Tolley, *Nature* **521**, 467–475 (2015).
3. D.-H. Kim *et al.*, *Science* **333**, 838–843 (2011).
4. S. Wang *et al.*, *Nature* **555**, 83–88 (2018).
5. D.-H. Kim *et al.*, *Nat. Mater.* **9**, 511–517 (2010).
6. Y. Liu *et al.*, *Nat. Biomed. Eng.* **3**, 58–68 (2019).
7. Y. Wang *et al.*, *Sci. Adv.* **3**, e1602076 (2017).
8. M. Park *et al.*, *Nat. Nanotechnol.* **7**, 803–809 (2012).
9. N. Matsuhisa *et al.*, *Nat. Mater.* **16**, 834–840 (2017).
10. T. Sekitani *et al.*, *Nat. Mater.* **8**, 494–499 (2009).
11. S. Choi *et al.*, *Nat. Nanotechnol.* **13**, 1048–1056 (2018).
12. Y. Kim *et al.*, *Nature* **500**, 59–63 (2013).
13. N. Matsuhisa, X. Chen, Z. Bao, T. Someya, *Chem. Soc. Rev.* **48**, 2946–2966 (2019).
14. E. J. Markvicka, M. D. Bartlett, X. Huang, C. Majidi, *Nat. Mater.* **17**, 618–624 (2018).
15. A. Fassler, C. Majidi, *Adv. Mater.* **27**, 1928–1932 (2015).
16. Z. Ma *et al.*, *Nat. Mater.* **20**, 859–868 (2021).
17. K. Parida *et al.*, *Nat. Commun.* **10**, 2158 (2019).
18. J. Wang *et al.*, *Adv. Mater.* **30**, e1706157 (2018).
19. S. Veerapandian *et al.*, *Nat. Mater.* **20**, 533–540 (2021).
20. S. Liu, D. S. Shah, R. Kramer-Bottiglio, *Nat. Mater.* **20**, 851–858 (2021).
21. Y. Lin *et al.*, *Nanoscale* **10**, 19871–19878 (2018).
22. S. Liu *et al.*, *ACS Appl. Mater. Interfaces* **10**, 28232–28241 (2018).
23. N. F. Uvarov, *Solid State Ion.* **136–137**, 1267–1272 (2000).
24. R. W. Style *et al.*, *Nat. Phys.* **11**, 82–87 (2015).
25. X.-Q. Zheng, H. Zhao, Z. Jia, X. Tao, P. X.-L. Feng, *Appl. Phys. Lett.* **119**, 013505 (2021).
26. G. M. Odegard, T. C. Clancy, T. S. Gates, *Polymer* **46**, 553–562 (2005).
27. N. Kazem, M. D. Bartlett, C. Majidi, *Adv. Mater.* **30**, e1706594 (2018).
28. K. S. Suslick, *Science* **247**, 1439–1445 (1990).
29. J. Kang, J. B.-H. Tok, Z. Bao, *Nat. Electron.* **2**, 144–150 (2019).
30. J. Kang *et al.*, *Adv. Mater.* **30**, e1706846 (2018).

ACKNOWLEDGMENTS

Funding: This study was supported by the National R&D Program funded by the Ministry of Science and ICT (grant no. NRF-2021M3H4A1A03048658), the Basic Science Research Program (grant no. NRF-2021R1C1C1011116), and the Wearable Platform Materials Technology Center (WMC, grant no. NRF-2022R1A5A6000846). This study was also partially supported by the National R&D Program (NRF-2021R1A4A1052070, NRF-2021M3H4A3A01050378, and NRF-2022M3E5E9017759) and 2020 Joint Research Project of Institutes of Science and Technology.
Author contributions: W.L., H.K., and J.K. conceived and designed the experiments. W.L. and H.K. prepared and characterized the LMP-based stretchable conductors. I.K. and J.-W.J. programmed the stretchable PPG sensor for signal conditioning circuit board demonstration. I.K. and W.L. fabricated the stretchable PPG sensor. W.L., H.K., H.P., H.L., J.S.P., and J.M.Y. performed scanning electron microscopy and transmission electron microscopy. J.J. and S.R. performed the computer simulations. W.L., H.K., and J.K. wrote the manuscript. All the authors discussed the results and commented on the manuscript. J.K. supervised this study.
Competing Interests: W.L., H.K., and J.K. are inventors in a patent application (Korean Patent application no. 10-2022-0036393, patent pending) that covers the formation of the LMP_{Net} in various polymers and their applications. **Data and materials availability:** All data are available in the main text or supplementary materials.

SUPPLEMENTARY MATERIALS

science.org/doi/10.1126/science.abo6631
Materials and Methods
Figs. S1 to S44
Tables S1 and S2
References (*31*–*48*)
Movies S1 and S2

Submitted 17 February 2022; accepted 23 September 2022
10.1126/science.abo6631

Science

Universal assembly of liquid metal particles in polymers enables elastic printed circuit board

Wonbeom LeeHyunjun KimInho KangHongjun ParkJiyoung JungHaeseung LeeHyunchang ParkJi Su ParkJong Min YukSeunghwa RyuJae-Woong JeongJiheong Kang

Science, 378 (6620), • DOI: 10.1126/science.abo6631

Acoustic patterning and fabrication

Liquid metals can be used to form the conductive pathways in a flexible matrix, but this approach requires patterning of the soft material and sintering of the liquid metal using lasers or mechanical force. Lee *et al*. used acoustic fields to assemble a network of liquid metal particles inside a polymer matrix for the fabrication of elastic printed circuit boards (see the Perspective by Qiao and Tang). Their devices showed high conductivity, high stretchability, strong adhesiveness, and negligibly small changes in electrical resistance during stretching. Because the acoustic field strategy is universal, the authors synthesized hydrogels, a self-healing elastomer, and photoresists by combining various polymers with liquid metals. —MSL

Science (ISSN) is published by the American Association for the Advancement of Science. 1200 New York Avenue NW, Washington, DC 20005. The title *Science* is a registered trademark of AAAS.